4.11

ANALYSIS OF TURBULENCE GENERATION BY GRAVITY WAVES WITHIN AN UPPER-TROPOSPHERIC FRONT

Steven E. Koch[1], Brian Jamison[1,2], Ed Tollerud[1], Cecelia Girz[1], Tracy Smith[1,2], Todd P. Lane[3], Ning Wang[1,2], Melvyn A. Shapiro[4], David D. Parrish[5], and Owen Cooper[6]

[1] *NOAA Research – Forecast Systems Laboratory, Boulder,Colorado*

[2]*In collaboration with the Cooperative Institute for Research in the Atmosphere (CIRA), Colorado State University, Ft. Collins, CO*

[3]*National Center for Atmospheric Research (NCAR)*

[4]*NOAA Office of Weather and Air Quality*

[5]*NOAA Research – Aeronomy Laboratory*

[6]*In collaboration with the Cooperative Institute for Research in Environmental Sciences (CIRES), University of Colorado, Boulder, CO*

1. Introduction

The vast majority of aircraft encounters with turbulence resulting in injuries, fatalities and occasional loss of aircraft have occurred above 20,000 ft (6.1 km), where clear-air turbulence (CAT) is the most probable cause. The generation of CAT is generally thought to be the product of microscale eddies arising from vertical shear instability within thin sheets of the atmosphere. To the extent that most of the energy associated with such eddies cascades down from the larger scales of atmospheric motion, and that the forecasts of the larger scales made from current numerical weather prediction models are sufficiently accurate, then the turbulence forecasting problem becomes one of identifying model predicted features *favorable* for the formation of microscale eddies. It is common practice to estimate turbulence associated with unresolved scales from model fields based on various approximations to the subgrid-scale turbulent kinetic energy (TKE) equation. Operational model guidance for forecasting turbulence known as the Graphical Turbulence Guidance (GTG) employs a multitude of algorithms computed from the Rapid Update Cycle (RUC) model (Sharman et al. 1999, 2002), all of which are based on some application of the shearing instability principle or the associated TKE generation concepts.

Aircraft measurements have shown wavelike structures with length scales of 2–40 km transverse to the flow at jet stream levels coexisting with turbulence (Shapiro 1978, 1980; Gultepe and Starr 1995; Demoz et al. 1998). Recent research indicates that gravity waves with wavelengths of 40–250 km may also play an important role in creating conditions conducive to the generation of turbulence immediately downstream of regions of diagnosed flow imbalance at jet stream levels (Koch and O'Handley 1997; Koch and Caracena 2002; Zhang 2004; Zhang et al. 2001). Imbalance in these studies was defined as a large residual in the sum of the terms in the nonlinear balance equation computed from mesoscale model fields.

It is unclear why such large-scale gravity waves should relate to observed reports of turbulence. The present case study sheds light on this perplexing question. First, we relate gravity waves to the structure of the jet/front system using special field observations and a combination of hydrostatic and cloud-resolving numerical model simulations. The field observations were collected on 17–18 February 2001 during the Severe Clear Air Turbulence Colliding with Aircraft Traffic (SCATCAT) experiment conducted over the Pacific Ocean. Second, this study examines relationships between turbulence intensity, aircraft-measured ozone fluctuations near the tropopause, and the structure of the upper-level jet. Spectral and wavelet analyses are conducted upon the aircraft in situ data to reveal relationships between the gravity waves and turbulence. For more information, the interested reader is directed to Koch et al. (2004) and Lane et al. (2004).

2. Experimental data and models

SCATCAT was designed to test the performance of RUC model predictors of turbulence and to improve understanding of turbulence generation mechanisms. The NOAA Gulfstream-IV (G-IV) aircraft collected flight-level and dropsonde data in a region extending

Corresponding author address: Steven E. Koch, NOAA/OAR/FSL, FS1, 325 Broadway, Boulder, CO 80305-3328; e-mail < Steven.Koch@noaa.gov>

from the core of an intense upper-level jet to its left exit region from ~2300 UTC 17 February to 0025 UTC 18 February 2001 (Fig. 1). The G-IV collected 25-Hz measurements along a stack of constant-altitude legs taken nearly perpendicular to the jet streak at altitudes of 12.5, 11.3, 10.7, and 10.1 km. Dropsondes launched at ~ 40-km intervals from the 12.5 km level were used to produce vertical cross-section analyses.

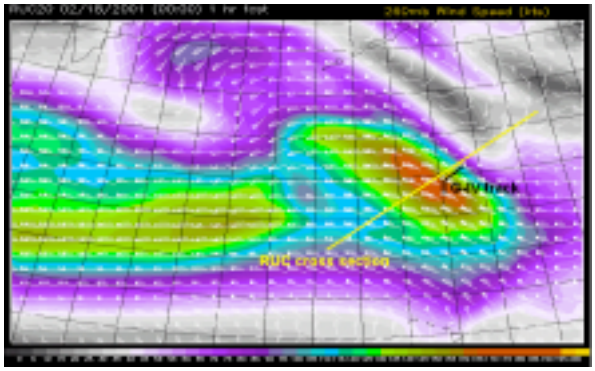

Fig. 1. RUC 1-h forecast of 33 000 ft (260 hPa) isotachs and wind barbs at 0000 UTC 18 February 2001 over the Pacific Ocean (note the Hawaiian and Aleutian Islands). Forecast maximum jet winds are 92 m s^{-1} vs. 100 m s^{-1} observed by the G-IV aircraft. Locations of RUC and G-IV vertical cross sections discussed below are shown. The G-IV aircraft flew from the core of this strong jet to its cyclonic side, and made three NE-SW stacked legs along the longest part of the flight lag perpendicular to the jet.

The RUC model was run with 20-km and 13-km resolutions and 50 hybrid isentropic-sigma levels in a manner closely mirroring the operational RUC model, except that the domain was shifted to the data-sparse central north Pacific and the AVN model supplied the RUC with boundary conditions instead of the Eta model. The operational RUC takes advantage of hourly updating with abundant data over the CONUS region, but the paucity of observations over the Pacific represented a challenge. In addition, a 1-km nested version of the Clark-Hall (CH) model was initialized at 0000 UTC 17 February. This nonhydrostatic model was used to study details of the turbulence generation process associated with the mesoscale gravity waves. Lane et al. (2004) present information about the CH model setup and results.

3. Tropopause undulations, gravity waves, turbulence, and ozone

The RUC model produced a rather deep tropopause fold within an intensifying upper-level frontal zone on the cyclonic side of the jet streak (Fig. 2). Also, several "tropopause undulations" can be seen. These features are actually upward-propagating gravity waves characterized by average horizontal and vertical wavelengths of 216 ± 66 and 1.8 ± 0.4 km, respectively. The waves propagated away from the local tropopause undulation areas. The CH model simulated comparable waves (not shown). Cross-section analyses computed from the dropsonde data (Fig. 3) also show vertically propagating mesoscale gravity waves in the region of strong vertical wind shear extending from the jet core into the lower stratosphere.

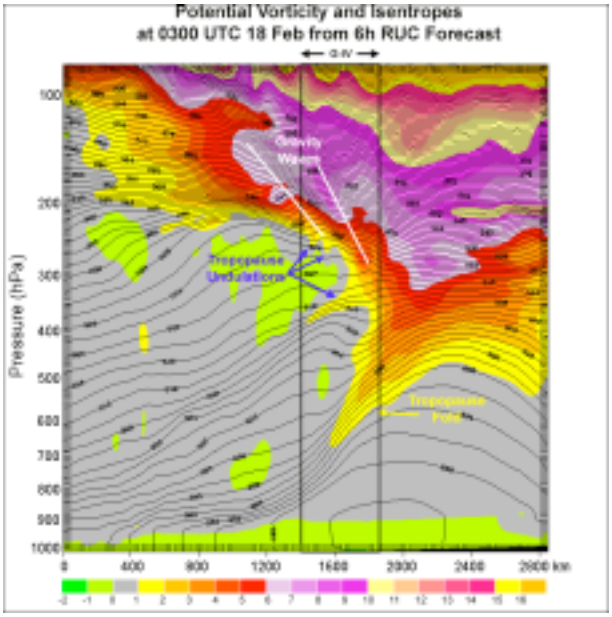

Fig. 2. Isentropic cross section of RUC 6-h forecast isentropic potential vorticity and potential temperature valid at 0300 UTC 18 February 2001. Parallel vertical lines denote segment over which G-IV aircraft took measurements, and for which the cross section in Fig. 3 is relevant. Note deep tropopause fold (>1.5 PVU) and tropopause undulations, above which occur vertically propagating gravity waves.

The DTF3 turbulence diagnostic algorithm (Marroquin 1998) is part of the suite of algorithms used by the GTG. DTF3 is based on the assumption that the dissipation rate of TKE is in steady state. An analysis of DTF3 from the dropsonde data (Fig. 3) indicates the likelihood of turbulence principally in three regions: the layer of strong vertical shear above the 100 m s^{-1} jet core, the shear layer directly beneath the jet core, and the region of strong shear and stability along the sloping warm frontal zone below 600 hPa. The G-IV did, in fact, encounter moderate or greater (MOG) turbulence in the uppermost of these regions on the three lower legs of the stack (yellow parts of the black flight segments).

Diagnosed MOG turbulence from the RUC model appeared in the same general regions (not shown). A comparison of the gradient Richardson number (Ri_g) computed from the RUC analyses that assimilated the dropsonde data with those that did not revealed similar patterns in Ri_g. However, in the absence of the dropsonde data, the RUC analysis of Ri_g (and DTF3, which is closely related to Ri_g) suffered, as considerably less area was covered by $Ri_g < 0.50$ (Koch et al. 2004).

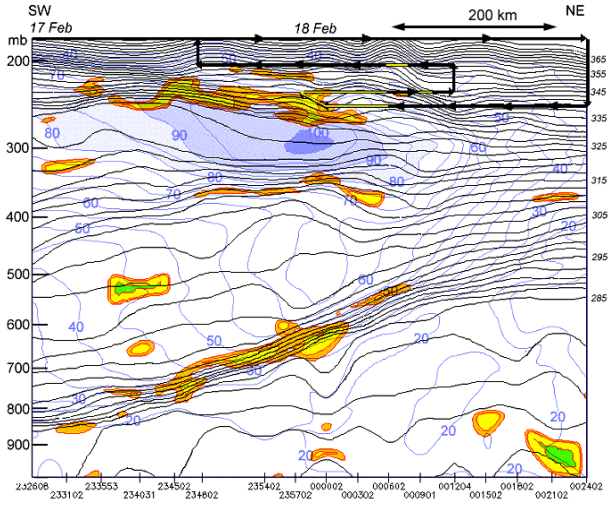

Fig.3. Vertical cross section of wind magnitude (blue lines, 5 m s^{-1} isotachs), potential temperature (black lines, 2K isentropes), and DTF3 computed from dropsondes. Jet core is highlighted by winds in excess of 80 m s^{-1} (maximum of 100 m s^{-1}), and DTF3 values are contoured at 0.6 and 1.0 m^2 s^{-3} (yellow and orange areas, respectively). The four legs of the G-IV are shown with black lines (arrows depict sense of aircraft travel). Those segments of the legs for which moderate-or-greater turbulence was diagnosed in the flight-level data are highlighted in yellow.

The strong association among the tropopause undulations, the gravity waves, DTF3-diagnosed turbulence and that actually detected by the G-IV above the jet is striking in the vertical cross sections. Equally intriguing is a banded nature to the DTF3 fields evident in horizontal displays. The diagnosed TKE (the DTF3 fields) in the RUC simulation appears as mesoscale bands at 33, 35, 37, and 39 Kft parallel to the general northwesterly wind regime (Fig. 4), and also parallel with a pronounced frontal zone just to their southwest. These bands developed with time in the model forecast.

Similar patterns of parallel bands, with a horizontal wavelength of ~180 km, appear in the TKE patterns in the 1-km resolution CH model (Fig. 5a). The upward propagating nature of the waves is manifested by the upwind slope to the bands of TKE, and even more prominently, the perturbation potential temperature in the vertical cross section display (Fig. 5b). This upward-propagating gravity wave behavior is similar to that displayed in the RUC isentropes (Fig. 2). According to the analysis conducted by Lane et al. (2004), these bands were the result of gravity wave modulation of the background shear and stability fields. The wave modulation of the mesoscale fields reduced the Richardson number near the wave crests and trough sufficiently to result in the generation of TKE, which relates directly to turbulence production.

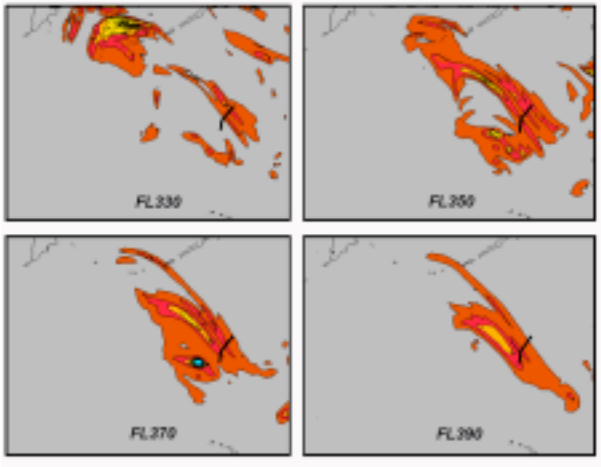

Fig. 4. Altitude variation of DTF3 forecast by RUC model for 0300 UTC (6-h forecast). Shown are the fields at 33-, 35-, 37-, and 39-Kft altitudes over the full model domain (note the Aleutian Islands to the north and the Hawaiian Islands to the south). The G-IV track is depicted by small, thick black line segment.

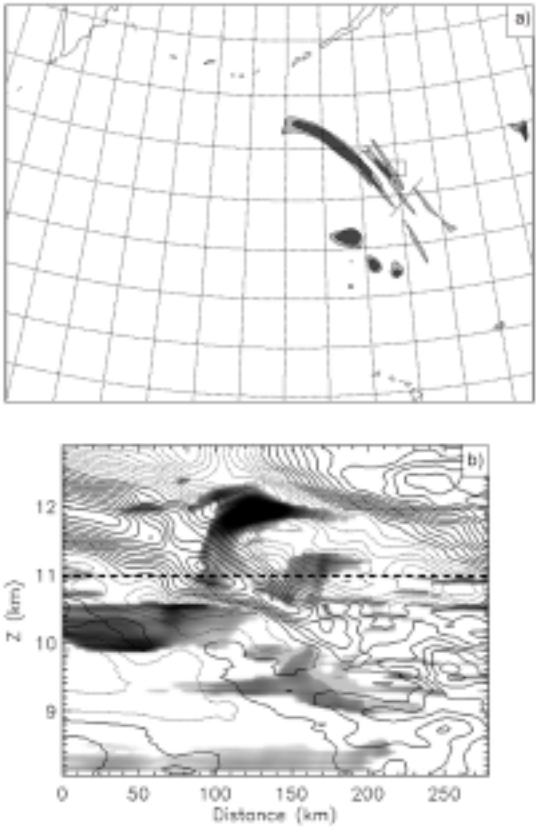

Fig. 5. a) Subgrid TKE at 11 km MSL at 0600 UTC from CH 1-km domain model and (b) cross section of subgrid TKE and perturbation potential temperature (0.5-K interval) fields from CH model along a southwest-northeast diagonal through the small box in (a). The shading is linear with the maximum value of 0.2 m^2 s^{-2} denoted by the darkest shade.

According to the analysis by Koch et al. (2004), the gravity waves were triggered in a region of highly unbalanced flow very near to the path of the G-IV aircraft (imbalance being defined as a large residual in the sum of the terms of the nonlinear balance equation). The imbalance was centered in the vicinity of the tropopause fold, where the lowest (and most pronounced) of the tropopause undulations joined with the primary fold (Fig. 2). Thus, the coexistence of multiple tropopause folds just ahead of a region of upper-level frontogenesis, jet stream imbalance, mesoscale gravity waves, and large TKE generation associated with turbulence production, appears to have been much more than just a coincidence.

Interrelationships between ozone and potential temperature fluctuations measured by the aircraft, and potential vorticity and potential temperature from the RUC model fields are quite interesting. A "pseudo-meteogram" method was developed for the purpose of comparing the model fields with the data collected by the aircraft traveling along a single line through the model domain, as explained by Koch et al. (2004). The results appear in Fig. 6 (at the 33 Kft flight altitude) and Fig. 7 (41-Kft altitude).

Stratospheric ozone levels on the order of 300–800 ppbv are seen in the layer between 33 Kft and 41 Kft. Ozone values are largest at the 41 Kft level (above the jet core), and at the northeast ends of both flight legs (the cyclonic side of the jet). This is consistent with the conjecture that the aircraft was penetrating a tropopause fold and entered or left the lower stratosphere in its northeast-southwest trek.

Potential vorticity and ozone act as passive tracers of air mass exchange processes. Fluctuations in aircraft measurements of ozone and potential temperature are highly correlated at 33 Kft (Fig. 6). The RUC potential vorticity and the aircraft ozone data both show a general trend downward as the aircraft approached the jet core from its cyclonic side, and both traces also indicate two large-scale rises in the time series, cresting at roughly 0039 and 0047–0050. The dropsonde cross-section analysis (Fig. 3) shows that the aircraft was penetrating a pronounced gravity wave at this time immediately to the northeast of the high DTF3 region (note that 33 Kft = 260 hPa). Close inspection of the G-IV time series in Fig. 6 also suggests the appearance of considerably greater high-frequency energy beginning at ~0046. In fact, the G-IV *in-situ* data indicated MOG turbulence beginning at this time (note the lowest-level yellow segment of the aircraft track in Fig. 3.)

Wild fluctuations in ozone and potential temperature were measured at the 41-Kft level, but these variables do not relate well to each other, nor to the RUC model variables (Fig. 7). Ozone and potential temperature observations at the intermediate flight altitudes (35 Kft and 37 Kft) bore a strong relationship with one another and with trends in the respective RUC model variables (not shown). As will be discussed next, turbulence was not reported on the 41-Kft flight leg, was quite pronounced at 33 Kft and 35 Kft, and was intermediate at 37 Kft. We take these facts to mean that the rapid fluctuations in ozone at 41 Kft indicate "fossil turbulence" from earlier stratosphere-troposphere exchange processes, whereas the fluctuations at lower levels represent currently active turbulence.

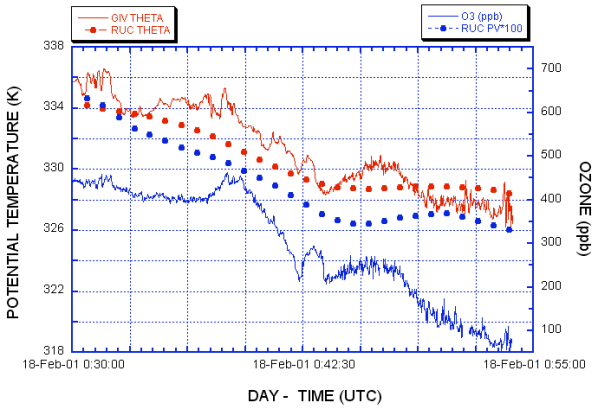

Fig. 6. Comparisons between in-flight measurements and RUC forecast of potential temperature for 33 Kft level for 0030–0055 UTC 18 February (red curve and red dots, respectively). In-flight measurements of ozone (blue curve) are also compared to RUC potential vorticity (blue dots). Potential vorticity values PV > 150 and ozone larger than 300 ppbv are stratospheric. The largest-scale fluctuations in the G-IV data are the mesoscale gravity waves with horizontal wavelengths ~100 km. Northeast is to the left (cyclonic side of the jet).

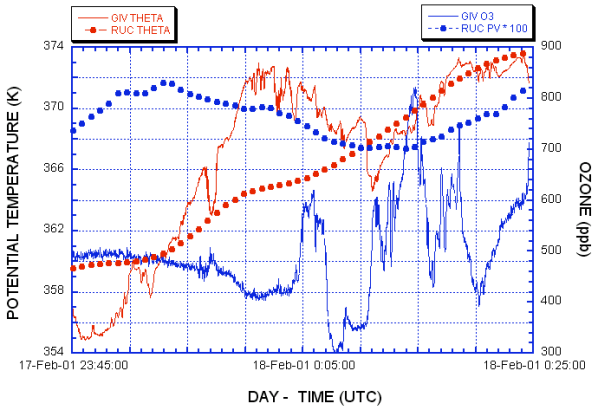

Fig. 7. Comparisons between in-flight measurements and RUC forecast fields at 41 Kft for 2345 UTC 17 February–0025 UTC 18 February. Aircraft flew in the opposite direction to that in Fig. 6, so northeast here is to the right.

4. Spectral and wavelet analyses

Composite time series from the four flight levels of 25-Hz aircraft vertical acceleration and 1-Hz vertical velocity data are shown by the red and blue traces in Fig. 8, respectively, for the entire 2340–0140 UTC period of G-IV observations. Both traces suggest that

negligible turbulence was encountered at the 12.5-km (41 Kft) flight level. MOG turbulence first appears at 0043 UTC at the 10.1 km (33 Kft) level and dominates the remainder of the record at that altitude and also at the 10.7 km (35 Kft) level. Last of all, a short burst of MOG turbulence from 0128–0131 UTC appears at the 11.4 km (37 Kft) level (this corresponds to 40 km spatial distance, given the aircraft true airspeed).

Fig. 8. Time series of turbulence variables showing onset of moderate or greater (MOG) turbulence at 0043 UTC and sporadic bursts of turbulence thereafter. Blue plot represents 1-Hz GPS Honeywell vertical velocity data, red plot is for the 25-Hz aircraft vertical acceleration data for the entire four flight legs of the mission, beginning at 12.5 km (41,000 ft), followed by legs at 10.1 (33,000 ft), 10.7 km (35,000 ft), and 11.4 km (37,000 ft).

Although these time series are suggestive of when turbulence is encountered, they do not directly provide information about the interactions between gravity waves and turbulence. For that purpose, the 25-Hz potential temperature, longitudinal (along-flight) wind, transverse (cross-flight) wind, and aircraft vertical acceleration data were subjected to an FFT spectral analysis. Only constant-altitude samples not containing abrupt changes in aircraft heading, pitch, and roll were used. The results showed that a significant spectral peak at 0.65 Hz (corresponding to a wavelength of 350 m) appeared only during the turbulent episodes. Cross-spectral analyses of the potential temperature and longitudinal wind data revealed a strong in-phase relationship (Koch et al. 2004), a result that is consistent with the polarization relation for gravity waves. The deduction from the auto- and cross-spectral analyses was the presence of gravity wave activity with wavelengths of 0.7–20 km at all four flight levels, though considerably less so at 41 Kft.

Spectral approaches do enable separation of waves from turbulence, but they are valid only in a "global" sense, because a sufficiently long record characterized by "statistical stationarity" is required. Since spectral analysis can only provide such nonlocal information, it is not well suited to the study of intermittent, nonstationary phenomena like turbulence, which displays rapid changes in phase, amplitude, and statistical properties. Direct observation of the turbulence generation mechanism, the intensity of the turbulence as a function of the wave amplitude, and its distribution in space and time is needed. Wavelet analysis is capable of resolving *localized* structures in the time-frequency domain. The wavelet transform coefficients provide information about both the amplitude and phase of the fluctuations at each time and frequency, and therefore, should be able to provide understanding of the *evolving* relationship between wave and turbulence characteristics.

Continuous wavelet analysis was applied to the horizontal wind, temperature, and vertical acceleration data obtained from the G-IV. For the transformation kernel function in the wavelet analysis, we used the continuous Morlet wavelet. The transform coefficients provide information about both amplitude and phase of the analyzed data (Fig. 9). An important issue can be addressed with wavelet analysis – the prediction from linear theory that the amplitude of the turbulence should be correlated with the amplitude of the progenitor gravity waves, such that the turbulence intensity oscillates with the wave period. The wavelet results were used to reconstruct the gravity waves in the f = 0.03–0.09 Hz band (wavelengths of 2.5–7.7 km). Comparison of the resulting analysis (Fig. 9c) to the time series of turbulent intensity in the 0.3–0.9 Hz band (wavelengths of 0.2–0.8 km) shown in Fig. 9d reveals in a direct way that *the times of occurrence of the strongest gravity wave amplitudes and the appearance of episodes of high turbulence energy were indeed highly correlated*. This behavior is particularly impressive during the extensive 0103–0110 UTC turbulence/wave episode (which extended for nearly 100 km). Closer inspection reveals that the higher-frequency gravity waves tended to occur in packets defined by wave envelopes of various sizes ranging from 7–20 km (Fig. 9e), and it is with these wave packets that the turbulence most strongly correlated.

During each gravity wave interval (defined by the period of time between successive wave troughs), the phase of the wave at which the maximum turbulent intensity occurred was plotted (Fig. 9b). Results indicate that turbulence intensity did not vary systematically with wave phase; thus, the wavelet analysis suggests that the wave-turbulence process involved both dynamic and convective instabilities.

The mechanism for turbulence production is related to non-linear advection, which causes the wave front to become steeper with increasing amplitude until it breaks, at which point energy flows from the primary wave into harmonics down to turbulence. Short-period gravity waves (in which the effects of the earth's rotation are negligible) display a linear polarization between the two components of horizontal perturbation winds (phase angle $\varphi = n\pi$, where n = 1, 2, …), as opposed to inertia-gravity waves, which display an elliptical polarization relationship. Lu et al. (2004) used this fact to reconstruct the waves in the current case in different frequency bands, by combining knowledge of the dominant wave frequencies obtained from the cross spectral analysis with the localized information from the wavelet analysis. That analysis confirms our conjecture that the gravity waves occurred in packets of 0.5–1.5-min duration (~7–20 km distance).

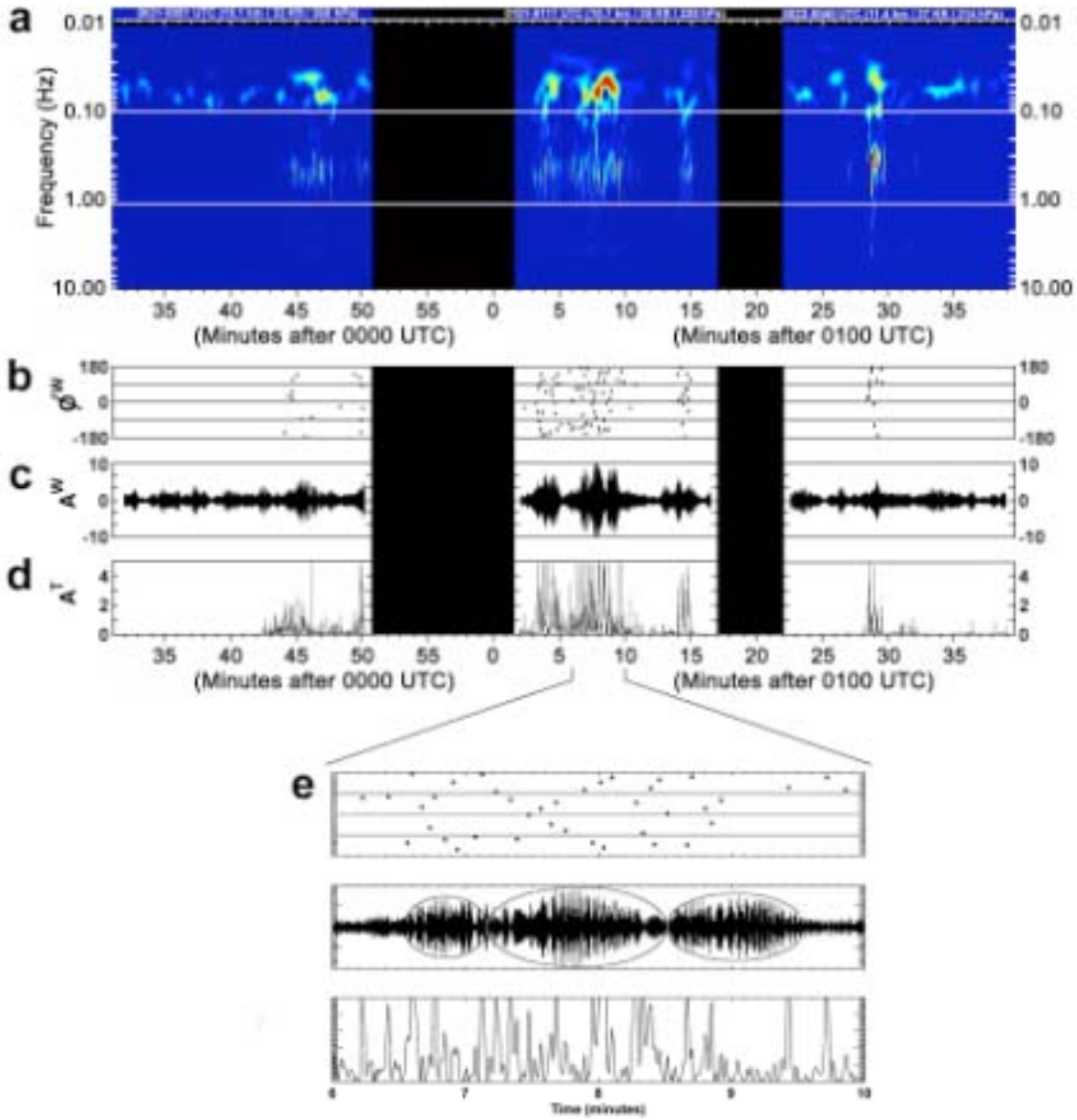

Fig. 9. Wavelet analysis of aircraft vertical acceleration data: (a) time-frequency display of wavelets (cm s^{-2}) at flight altitudes of 10.1, 10.7, and 11.4 km; (b) phase φ_w of gravity waves (degrees) at which maximum turbulence intensity occurred (only if larger than 0.5 cm^2 s^{-4}); (c) amplitude A_w (cm s^{-2}) of gravity waves reconstructed from wavelet analysis for the 0.06–0.09 Hz frequency band; (d) turbulence intensity A_T (cm^2 s^{-4}) at a frequency of 0.65 Hz; and (e) zoomed-in display of panels b, c, d for the period 0106–0110 UTC showing three wave packets (envelopes) by the ellipses. Background noise level of wavelet amplitudes is depicted in blue in panel a, with increasing intensity shown in yellow and red shading (contributions at frequencies greater than 1 Hz have been filtered out of this display). Black segments indicate times when the aircraft was going through maneuvers (primarily changes in altitude).

5. Conclusions

Dropwindsonde and in-situ data collected by the NOAA G-IV research aircraft during the SCATCAT case of 17–18 February 2001 and simulations from a variety of numerical models offered an unprecedented opportunity to study the relationships between clear-air turbulence and mesoscale aspects of upper-level jet/frontal systems. The major conclusion drawn from this study is that moderate or stronger turbulence occurred in direct association with a wide spectrum of gravity waves spawned within a developing frontal zone on the cyclonic shear side of an intense upper-level jet streak. Our results support the growing evidence that upper-level frontal zones are prolific producers of gravity-inertia waves, which propagate upward into the lower stratosphere from their origins within the highly sheared region just above the tropospheric jet stream.

Other interesting discoveries were made in the course of this study. First, the gravity waves emanated from a secondary tropopause fold that formed along a

stable lamina above the primary fold. Second, this region was highly unbalanced, suggesting that the source of the largest-scale gravity waves (displaying horizontal wavelengths of 200–250 km and wave vectors normal to the northwesterly upper-level flow) may have been from geostrophic adjustment. Third, this same region was also the source for a wide spectrum of higher-frequency gravity waves detected in the spectral and wavelet analyses of the 25-Hz in-flight data (with wavelengths of 1–20 km). Fourth, the intensity of turbulence was highly correlated with packets of gravity waves with these characteristics, and within each envelope existed even smaller-scale gravity waves.

In summary, the resultant picture presented by a synthesis of these findings is one of a cascade of different wavelength phenomena, starting with the inertia-gravity waves associated with the flow imbalance, proceeding through the generation of higher wavenumber phenomena, and ending with excitation of Kelvin-Helmholtz instabilities at the smallest scales.

Turbulent regions diagnosed from the RUC model forecasts and TKE fields forecast by the nonhydrostatic CH model both displayed a strongly banded behavior associated with the gravity waves parallel to the upper-level front. Turbulence was generated as the gravity waves perturbed the background wind shear and stability, promoting the development of bands of reduced Richardson number conducive to the generation of turbulence. The DTF3 turbulence diagnostic computed from the operational RUC model constitutes an important piece of information for the current automated turbulence-forecasting algorithm (GTG). Our results suggest the value of the DTF3 approach, but also indicate that other algorithms should be developed to account for the degree of imbalance, such as proposed by Koch and Caracena (2002), since inertia-gravity waves appear to play an important role in modifying the environment to be more susceptible to shearing instability. In addition, evidence was presented showing that the computation of Richardson number-related fields such as DTF3 is quite sensitive to the existence of high quality mesoscale data, such as the dropsonde data available for this study.

Another conclusion drawn from this study is that ozone cannot be used as a substitute for more direct measures of turbulence and that “fossil turbulence” from earlier events may have existed. This finding needs to be more fully evaluated in other case studies employing multiple aircraft equipped to measure the vertical distribution of ozone, such as from airborne lidar systems. There is also a need to conduct idealized studies of the wave scale cascade process indicated by our analyses, as this process is not well understood.

6. Acknowledgments

The authors express their appreciation to C. Webster at NCAR for assistance with the spectral analysis, to J. Parrish at the NOAA Aircraft Operations center for guidance in the proper use of the aircraft data, and to F. Caracena for analysis of unbalanced flow. Reviews of this manuscript were kindly provided by F. Caracena and N. Fullerton. This research is in response to requirements and funding by the Federal Aviation Administration (FAA). The views expressed are those of the authors and do not necessarily represent the official policy or position of the FAA.

7. References

Demoz, B. B., D. O’C. Starr, K. R. Chan, and S. W. Bowen, 1998: Wavelet analysis of dynamical processes in cirrus. *Geophys. Res. Lett.*, **25,** 1347–1350.

Gultepe, I., and D. O’C. Starr, 1995: Dynamical structure and turbulence in cirrus clouds: aircraft observations during FIRE. *J. Atmos. Sci.,* **52,** 4159–4182.

Koch, S. E., and C. O’Handley, 1997: Operational forecasting and detection of mesoscale gravity waves. *Wea. Forecasting*, **12,** 253-281.

Koch, S. E., and F. Caracena, 2002: Predicting clear-air turbulence from diagnosis of unbalanced flow. Preprints, *10th Conference on Aviation, Range, and Aerospace Meteorology*, Portland, OR, Amer. Meteor. Soc., 359-363.

Koch, S. E., et al., 2004: Turbulence and gravity waves within an upper-level front. *J. Atmos. Sci.* (submitted).

Lane, T. P., J. D. Doyle, R. Plougonven, M. A. Shapiro, and R. D. Sharman, 2004: Observations and numerical simulations of inertia-gravity waves and shearing instabilities in the vicinity of a jet stream. *J. Atmos. Sci.* (in press).

Lu, C., S. E. Koch, and N. Wang, 2004: Determination of temporal and spatial characteristics of atmospheric gravity waves combining cross-spectral analysis and wavelet transformation. *J. Geophys. Res.* (in press).

Marroquin, A., 1998: An advanced algorithm to diagnose atmospheric turbulence using numerical model output. Preprints, *16th Conf. on Weather Analysis and Forecasting*, Phoenix, AZ, American Meteor. Society, 79-81.

Shapiro, M. A., 1978: Further evidence of the mesoscale and turbulence structure of upper level jet stream-frontal zone systems. *Mon. Wea. Rev.*, **106,** 1100–1111.

Shapiro, M. A., 1980: Turbulent mixing within tropopause folds as a mechanism for the exchange of chemical constituents between the stratosphere and the troposphere. J. *Atmos. Sci.,* **37,** 994–1004.

Sharman, R.C., C. Tebaldi, and B. Brown, 1999: An integrated approach to clear-air turbulence forecasting. Preprints, *8th Conf. on Aviation, Range,*

and Aerospace Meteorology, Dallas, TX, Amer. Meteor. Soc., 68-71.

Sharman, R, C. Tebaldi, J. Wolff, and G. Wiener, 2002: Results from the NCAR Integrated Turbulence Forecasting Algorithm (ITFA) for predicting upper-level clear-air turbulence. Preprints, *Tenth Conf. on Aviation, Range, and Aerospace Meteorology*, 351–354. Amer. Meteor. Soc., Portland, OR.

Zhang, F., S. E. Koch, C. A. Davis, and M. L. Kaplan, 2001: Wavelet analysis and the governing dynamics of a large-amplitude mesoscale gravity wave event along the East Coast of the United States. *Quart. J. Roy. Meteor. Soc.,* **127,** 2209-2245.

Zhang, F., 2004: Generation of mesoscale gravity waves in upper-tropospheric jet-front systems. *J. Atmos. Sci.,* **61,** 440–457.